Climate and Natural Radon Levels in Castleguard Cave, Columbia Icefields, Alberta, Canada

T. C. Atkinson, P. L. Smart & T. M. L. Wigley

CLIMATE AND NATURAL RADON LEVELS IN CASTLEGUARD CAVE, COLUMBIA ICEFIELDS, ALBERTA, CANADA*

T. C. ATKINSON
Climatic Research Unit and School of Environmental Sciences, University of East Anglia Norwich NR4 7TJ, England, U.K.

P. L. SMART
Department of Geography, University of Bristol, Bristol BS8 1SS, England, U.K.

T. M. L. WIGLEY
Climatic Research Unit and School of Environmental Sciences, University of East Anglia Norwich NR4 7TJ, England, U.K.

ABSTRACT

Castleguard Cave has a climate dominated by chimney-effect winds, due to temperature differences between interior and exterior air. A theory is developed relating the magnitude of winds to these differences and to friction at cave walls. Friction factors derived are the first for cave conduits, and agree with values expected from wall roughness and known values from mines.

Radon-222 content of air and waters indicates that radon is added to cave air by exhalation, direct emanation, and diffusion from cracks in rock around principal passages. Radon dilution in the central cave is attributed to tributary air currents from larger fissures. These results demonstrate that the cave is embedded in a porous medium which has a significant influence on air flows.

Temperature profiles demonstrate geothermal heating of the central cave. Isotherms on a cross section of Castleguard Mountain indicate that conductive heat flow to the base of the Columbia Icefield is substantially less than to adjacent ice-free areas, due to abstraction by meltwaters percolating downwards from the ice.

Relative humidity and vapor pressure profiles show rapid increases of water content in dry air blowing into the entrance, as predicted by theory. In the central cave, temperature and vapor pressure profiles reflect heat and moisture exchange with the walls. These predominate over adiabatic effects. Evaporation amounts to a few millimeters of water per year.

INTRODUCTION

The climate of Castleguard Cave has three particularly interesting features. These are the chimney-effect winds which blow through it, the thermal regime in which the core of the cave beneath the Columbia Icefield is heated geothermally, and the heat transfer, evaporation, and condensation occurring along the principal passage. The fairly simple plan and airflow patterns also afford an opportunity to study the emanation of radon gas from

---

*A version of this paper was presented orally at a symposium, "Karst and Caves of Castleguard Mountain," at the 8th International Congress of Speleology, Bowling Green, Kentucky, U.S.A., 20 July 1981.

TABLE 1
Estimated mean temperatures (°C) at Castleguard Cave entrance (1970 m a.s.l.)

J	F	M	A	M	J	J	A	S	O	N	D	Year
-19.4	-13.9	-9.9	-2.8	2.7	6.2	8.9	7.8	3.3	-2.3	-10.1	-15.2	-3.7

the cave walls into the air, and to use the patterns of radon activity to detect tributary currents of air.

There are no systematic records of climatic conditions close to the entrance to Castleguard Cave. The nearest meteorological station lies over 100 km away. Mean monthly and mean annual temperatures at the cave entrance have been estimated using available meteorological station records from a region around Castleguard, approximately 114 to 120°W and 50 to 54°N. They are believed to be accurate to within ±1°C and are shown in Table 1.

AIRFLOW AND RADON CONCENTRATIONS

THEORY OF CHIMNEY-EFFECT WINDS IN CAVES

Chimney-effect winds have been described in general terms by Wigley and Brown (1976). They occur in caves with two or more entrances at different heights, where the temperature of air inside is different from outside. The pressure exerted at the lowest entrance by the column of air inside the cave will differ from the pressure of the external air because the density of the air depends upon temperature. The pressure difference, Δp, at the lower entrance of the simple cave in Figure 1 is determined by the mean densities of the air columns,

$$\Delta p = (\bar{\rho}_{int} - \bar{\rho}_{ext})gh = (\Delta\bar{\rho})gh \qquad (1)$$

where the subscripts int and ext refer to the mean internal and external air densities, respectively, g is the acceleration due to gravity, and h is the elevation difference between the upper and lower cave entrances. The air density is related to the virtual temperature,[1] T^*, by

$$\rho = \frac{p}{R_d T^*} \qquad (2)$$

where R_d is the specific gas constant for dry air. Combining these equations, we have

$$\Delta p \approx -gh \frac{\bar{\rho}_{int}}{\bar{T}^*_{ext}} \Delta \bar{T}^*. \qquad (3)$$

The bars indicate averages over the height range of the cave and $\Delta \bar{T}^* = \bar{T}^*_{int} - \bar{T}^*_{ext}$. The approximation involved here is dependent on h, but is excellent for $h \le 1000$ m. Since $\bar{\rho}_{int}$ is approximately constant relative to changes in $\Delta \bar{T}^*$, the pressure differential driving force for chimney effect winds depends largely on the temperature differ-

ence between the cave and outside, expressed as a fraction of the absolute temperature in °K. When the cave air is colder than the outside air ($\Delta \bar{T}^* < 0$) the pressure exerted by the cave air will be greater than the pressure outside ($\Delta p > 0$) and the wind will blow out of the lower entrance. When outside conditions are colder, the wind will blow inwards and upwards.

Since air temperatures in caves are usually nearly constant, while external temperatures vary, we may expect chimney-effect winds to reverse direction seasonally and also to reverse daily at some times of the year.

Equation 3 is based on a hydrostatic argument. When the air is moving there is in fact no abrupt pressure change at the lower entrance, but a gradual drop in pressure between the two ends of the cave. If we neglect the changes in kinetic energy, gravitational potential, and air density, all of which are small, then the pressure drop Δp can be equated to the frictional head loss along the cave, using the well-known Darcy-Weisbach equation for turbulent flow in pipes.

$$|\Delta p| = \frac{f L V^2 \bar{\rho}_{int}}{8R} \qquad (4)$$

where f is the friction factor, L the cave length, V the average windspeed, and R the hydraulic radius ($R =$ Area/Perimeter). Substitution and rearrangement gives

---

[1] The virtual temperature is the temperature of dry air with the same density as the moist air under consideration. Since $T^* \approx T$, relatively little error will be introduced by using the dry bulb temperature in practice.
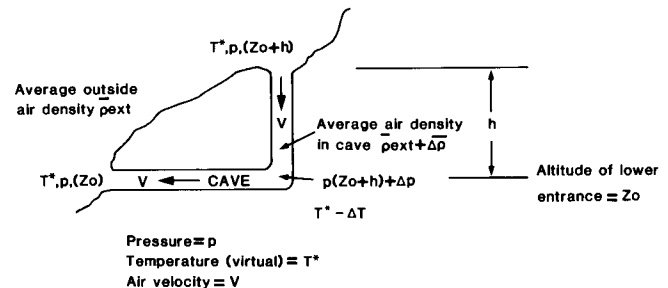
FIGURE 1. Chimney-effect wind in a simple cave.

the speed of the cave wind as a function of temperature conditions, the hydraulic radius, height range, and length of the cave.

$$V_2 \approx \frac{8Rg}{f} \cdot \frac{h}{L} \cdot \frac{|\Delta \bar{T}^*|}{\bar{T}^*_{ext}} \tag{5}$$

Note that this equation applies to steady, uniform flow. Error will be introduced if it is applied to rapidly changing conditions, but such errors are no worse than other uncertainties in the formulation.

The factor f in equation (4) is the flow resistance and is, in general, a function of the Reynolds Number (N_R) of the flow and the roughness of the cave walls relative to the hydraulic radius (Streeter, 1971:569ff.). For large N_R, the Reynolds Number dependence is small. For caves with a hydraulic radius ~ 1 m and kinematic viscosity of air of 1.4×10^{-5} m^2 s^{-1}, winds of greater than 0.14 m s^{-1} will have $N_R > 10,000$, in which case f depends only upon the relative roughness, and is given by

$$\frac{1}{\sqrt{f}} = 2.03 \log \frac{aR}{k} \tag{6}$$

where a is a constant equal to 13.46 for circular pipes and k is the height of projections from the wall which are usually from one-hundredth to one-tenth of the passage diameter. Thus, R/k will be about 2.5 to 25, and we should expect reasonably straight cave passages to have $f \approx 0.04$ to 0.10.

There are no reliable measurements of f from caves reported in the literature. McElroy (1966) gives f for rock walled and timbered mine galleries as being in the range 0.03 to 0.22. The upper end of this range refers to sinuous galleries in igneous rocks or with timber props, which are probably comparable in their effects to the rather rough cave walls considered above.

Constrictions in pipes are well known to exert a large effect upon flow resistance. Consider a cave with two sections of length L, and hydraulic radius R_1 connected by a smaller passageway L_2 with hydraulic radius R_2. If all sections have the same *relative* roughness, they will have equal values of f and the pressure drop will be

$$\Delta p = \frac{f \bar{\rho}_{int}}{8} \left(\frac{2V_1^2 L_1}{R_1} + \frac{V_2^2 L_2}{R_2} \right) \tag{7}$$

Since

$$V_1 R_1^2 = V_2 R_2^2 \tag{8}$$

$$\Delta p = \frac{f \bar{\rho}_{int}}{8} \frac{2V_1^2 L_1}{R_1} \left\{ 1 + \frac{1}{2} \frac{L_2}{L_1} \left(\frac{(R_1)}{R_2} \right)^5 \right\} \tag{9}$$

Equation 9 shows that the effect of hydraulic radius differences is expressed as a fifth power and has a profound effect on the cave wind speed, V_1. For example, if $L_1 = 10 L_2$ and $R_1 = 4 R_2$ the term in brackets is equal to 52.2.

For given pressure drop, V_1, the wind speed through the large radius part of the cave, is roughly 7 (i.e., $\sqrt{52.2}$) times slower than it would have been through a cave with no constrictions. If one assumed there were no constrictions, then the speed would be interpreted as a substantially larger ($52\times$) friction factor. Constrictions due to crawlways, sediment accumulations, and boulder chokes are common in caves and may lead to the apparent value of f for a whole system being much higher than any of the true values for individual sections. Constrictions may account for the very large apparent values of $f \approx 30$ to 150 determined from water flow in phreatic caves by Atkinson (1977).

AIRFLOW IN CASTLEGUARD CAVE

Topographic and morphologic characteristics of Castleguard Cave are summarized by Ford et al. (1983, this symposium).

The mean internal air temperature of the cave is 2.4°C, and it is believed that seasonal departures from this are very small. A vigorous draught normally blows through the entire length of the main passage, reversing direction between summer and winter, as expected from equation 3. The second, higher entrance is not known but is believed to consist of cave passages, shafts, or fissures connected with crevasses in the Columbia Icefield. From the temperature data of Table 1, and taking into account the 350-m height range of the known cave, the wind may be expected normally to blow into the cave in winter, reverse direction around April to June and blow outwards until reversing again in August to October. This is in fact the general pattern observed from repeated visits to the entrance by various groups over the last 15 yr. In spring and autumn, when cave and mean external temperatures are nearly equal, the diurnal fluctuations of outside temperature may produce reversals, as may temperature changes associated with synoptic-scale weather systems. Short-term reversals lasting between a few hours and a couple of days have been observed in October 1970 (by J. M. Boon) and in April 1980.

Air velocities and discharges were measured by fan anemometer at measured cross sections in April 1972 (M. C. Brown) and in April 1979 and 1980 by the authors. Results are shown in Table 2 and Figure 2. In 1979 the 11 measurements were spread over the first 4 km of the cave but showed no systematic trend with distance from the entrance. In 1980 measurements were made up to 8 km from the entrance (Figure 2). Despite a wide scatter, they suggest that airflow increases inwards from the entrance, by approximately 0.14 m^3 s^{-1} km^{-1}, or 19% of the discharge at the entrance for each kilometer distance into the cave. A diurnal effect may be seen in the difference between morning and evening airflow near Camp I (the Grottoes, 5 km from entrance) and at Camp II (the Crutch, almost 8 km from the entrance).

Friction factors calculated from the air discharge data using equation 5 are presented in Table 2, column 5. Because the discharge increased into the cave, calculations using the airflow close to the entrance, such as that

TABLE 2

TABLE 2
Airflow measurements and calculated friction factors

Date	Mean air discharge (m^3 s^{-1})	Number of measurements	Mean external temperature (°C)	Apparent[a] friction factor (f)	Estimated[b] true friction factor
1973	1.9	1	-7.8	2.31	0.90
1979	2.5	11	ca. -10	1.56	0.60
1980	1.3[c]	7	1.5	0.87	0.33
1980	0.8[d]	2	1.5	2.28	0.87

Mean cross section = 10.4 m^2 (n = 41); h = 350 m.
[a]L = 10,000 m; R = 0.7 m.
[b]L_1 = 5000 m; L_2 = 500 m; R_1 = 0.7 m; R_2 = 0.35 m.
[c]All air discharge data.
[d]Entrance discharge only.

for 1973, will overestimate the value of f. This is illustrated by the last two lines of Table 2 which compare f calculated from the average discharge over the whole cave with the higher value obtained from the discharge at the entrance. Overall, f appears to be in the range 0.8 to 2.3 for the cave as a whole which is somewhat higher than expected. This is the apparent value based upon an assumed constant hydraulic radius of 0.7 m (see footnote to Table 2). In fact the cave contains lengthy crawlways near the entrance and at its far end, with shorter crawls in the Grottoes and Holes-in-the-Floor areas. Applying equation 9, while not precise for an airflow which increases downstream, suggests that 500 m of crawlway with R = 0.35 m in a total length of 10,500 m with R = 0.7 m would have the effect of increasing the apparent value of f by 2.6 times (last column of Table 2). It seems likely, therefore, that the somewhat high apparent values of f in Table 2 are exaggerated by constrictions, and the true value for the cave passages is in the range 0.3 to 0.9 (or less if there were more constrictions). This is higher than both the range expected from relative roughness, and the values for moderately obstructed and sinuous mine galleries. The discrepancy may be due to poor estimation of the extent of constrictions, especially in the unexplored part of the cave, or to the sinuosity of the cave passage.

This simple analysis suggests that Castleguard Cave obeys rather well the simple theory of chimney-effect winds outlined above. However, the downflow increases in air discharge observed in 1980 indicates that a view of the cave as a simple conduit with constant flow rate is an over-simplification. Further insight into the complexity of the true situation can be obtained from a study of natural radon levels, described in the next section.

RADON ACTIVITY AND AIRFLOW
Measurement and Results

Radon-222 occurs in the air of caves and mines as a result of radioactive decay of trace amounts of radium in the rocks of the walls or in sediments, followed by diffusion of the radon gas into the cave atmosphere. Radon
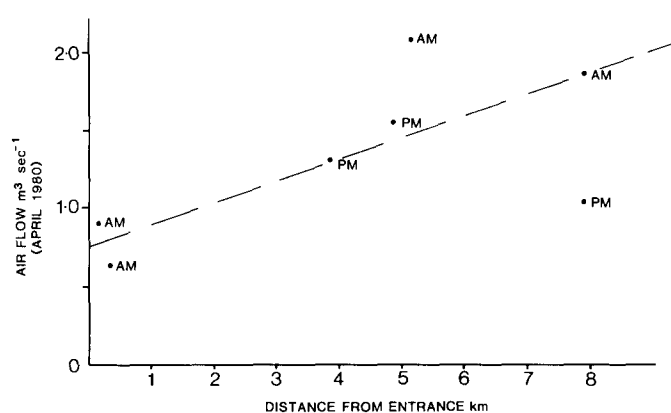
FIGURE 2. Air discharge as a function of distance from the entrance, Castleguard Cave, April 1980. AM = measurement in morning, PM = measured in evening.

may also be present in small inflows of water from which it is released by degassing. Radon-222 has a half-life of 3.83 d and very low concentrations can be detected by measuring the alpha particle activity of air samples. Radon concentrations of nine samples of air in Castleguard Cave were measured in the field using a portable alpha-counter designed for the monitoring of radiation levels in mines (EDA Instruments Inc., RDA-200 portable radon detector). Concentrations all lay in the range 1 to 10 pCi L^{-1}.

A second method of monitoring [222]Rn has been developed by Smart (unpublished). Briefly, the method consists of exposing small (1.5 × 7 cm) strips of clear CR-39 plastic sheet (Pershore Mouldings Ltd., U.K.) to the air for periods of several days. Alpha-particles emitted by disintegrations near the surface of the strips will damage the plastic, forming tracks which may later be revealed as microscopic pits by etching with alkali (Henshaw et al., 1979). The relative level of radioactive dose to which the strip has been exposed can be expressed by the numbers of tracks per square millimeter. Average dose rates can be compared between strips as tracks per

square millimeter per hour of exposure. When supplied, the plastic sheet is covered on both sides by a Mylar film, which may be peeled off to expose the surface of the plastic. For the Castleguard study, the protective films were removed a few days before field work began. One side of the plastic was covered with a piece of glass-fiber filter paper (Whatman GF/A), taped tightly to its surface, and the other was left exposed. Because ^{222}Rn is a gas, it can easily diffuse through the filter paper and its disintegrations will be recorded as tracks on the plastic surface beneath. The other sources of radioactivity in the air are particulate aerosols of ^{218}Po, ^{214}Pb, ^{214}Bi, and ^{214}Po, all derived from decay of ^{222}Rn. These particulates will lodge on the outer surface of the filter paper and their disintegrations will not damage the plastic surface. The prepared strips were stored immediately in sealed polythene bags and transported to the cave. At each monitoring site a single strip was removed from its bag and suspended for several days in the middle of the passage on a nylon monofilament. The strips were recovered and resealed into bags, the total exposure time being recorded. On return to the laboratory the filter paper was removed and the strips were etched for 6 h in 6M NaOH at 75°C. The tracks on the filter paper covered side of the strips were then counted at a magnification of ×200.

In the Castleguard study we recorded the track density on exposed strips and on control strips which were taken into the cave but not removed from their bags. The densities on control strips were found to be significant because of alpha particles emitted from the filter paper in contact with the plastic surface. The rate of track production due to this cause was an order of magnitude lower than that due to exposure to the cave atmosphere (0.141 × 10^{-2} tracks mm^{-2} h^{-1}). This nonradon background was subtracted from the measured track densities.

The background-corrected track density on the screened side of the plastic strips is compared with point measurements of ^{222}Rn concentration in Figure 3a. In spite of large counting errors, the correlation is very close and the best-fit line shows a simple proportionality between the two measures of radon activity. This is perhaps surprising when it is remembered that the cave wind was fluctuating diurnally and the gas samples were taken at arbitrary times. Possibly the closeness of the correlation indicates that radon concentrations did not fluctuate very greatly as the wind strength altered. The plastic strips were in place for several days and we may expect that diurnal fluctuations in the wind affected them all to a roughly similar degree. A puzzling feature of Figure 3a is the nonzero intercept of the regression. Since all the control detectors and a few of the exposed detectors showed track densities far smaller than the intercept value it seems possible that the relationship between track density and radon concentration is strongly curvilinear at extremely low radon levels, though the reason for this is not known.

Figure 3b shows the profile of radon track densities

recorded over the length of the cave during 5 d in April 1980. Track densities and, by implication, radon concentrations vary irregularly, with very low values at sites close to water inlets from the roof (Waterfall Rooms in First and Second Fissures, A62 shaft, Crutch) or where there are fissure passages leading off the main passage (P24 shaft, the Alley). Between such sites as these, radon levels are higher, showing a rapid increase in the first 2600 m of the cave, followed by a long decline to a minimum around 6300 to 7200 m. In the final 1500 m before the end of the known cave, radon levels increase somewhat, to a track density of 9 × 10^{-2} mm^{-2} h^{-1}.

Discussion

In the foregoing description of airflow, Castleguard Cave was treated as if it were a simple tube with constant cross section and air velocity. Under steady conditions the radon activity at any distance, x, from the entrance of such a tube is given by

$$A(x) = \frac{A_w}{\lambda}(1 - e^{-\lambda x/V}) \tag{10}$$

where V is the velocity of the air, λ the decay constant of ^{222}Rn, and A_w the rate of addition of radon to the air from the cave walls in concentration units per unit time. The air at the entrance is assumed to have zero radon activity. Note that, since λ is small, $A(x)$ should be a linearly increasing function of x for $x \leq (V/2\lambda) \approx$ 30,000 m. The solid line in Figure 3c shows that the radon levels increase rapidly at first, then more slowly, to a plateau at which the rate of addition of radon is just balanced by its decay. The rate of approach to plateau conditions can be defined by a relaxation distance, x_0, which is the distance which air must travel before the difference between its activity A and the plateau value declines to $1/e$ of its initial value. The relaxation distance is $x_0 = V/\lambda$. For Castleguard, $V \approx 450$ m h^{-1} and $\lambda = 0.0075$ h^{-1}, so $x_0 \approx 6.0 × 10^4$ m, about seven times longer than the cave itself. Thus the expected pattern if Castleguard were a simple tube would be a fairly steady increase in radon activity along its length, with no sign of a plateau. This is not the pattern observed in Figure 3b. Only in the first 2600 m does the expected behavior occur, and even there it is punctuated by a low value at the P24 shaft.

Both the irregular decreases of radon activity and the longer general decline from the First Fissure to the Crutch are interpreted as being due to tributaries of air which have a lower radon content than the cave air. This is strongly supported by the very low activity of air in the A62 invasion water shaft, a side passage from which a draught blows, and the corresponding depression of radon activity at the entry point of this air into the main cave (see tied points of Figure 3b).

A single tributary entering a tube of constant cross section at x_1 would increase the velocity from V_0 to V_1.
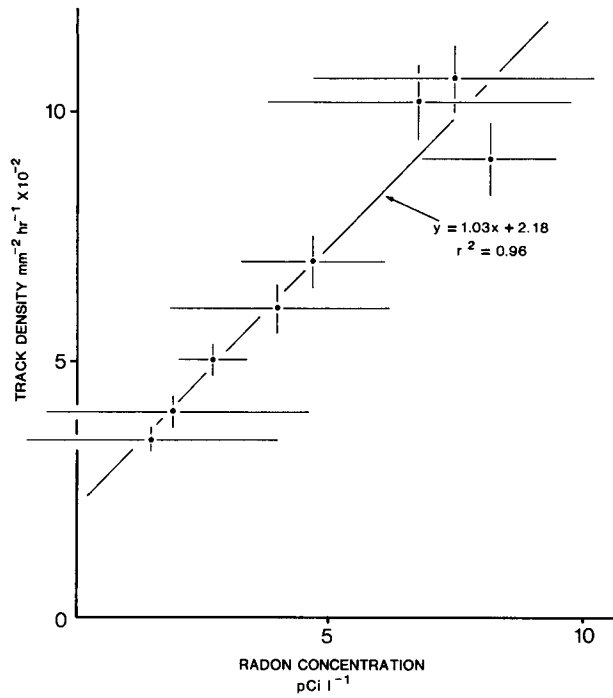
A. Comparison of direct measurement on air samples with track density on plastic strip detectors. Error bars are ±1σ
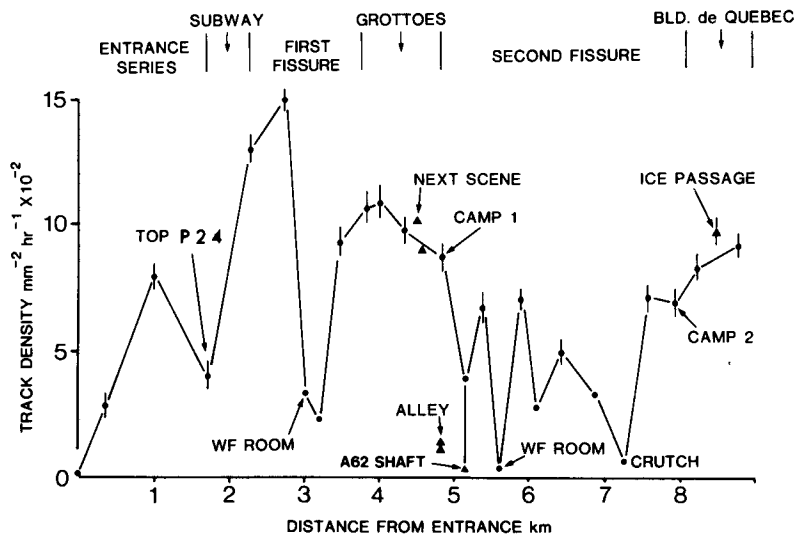
B. Variation of radon activity with distance from the entrance. Error bars are ±1σ.
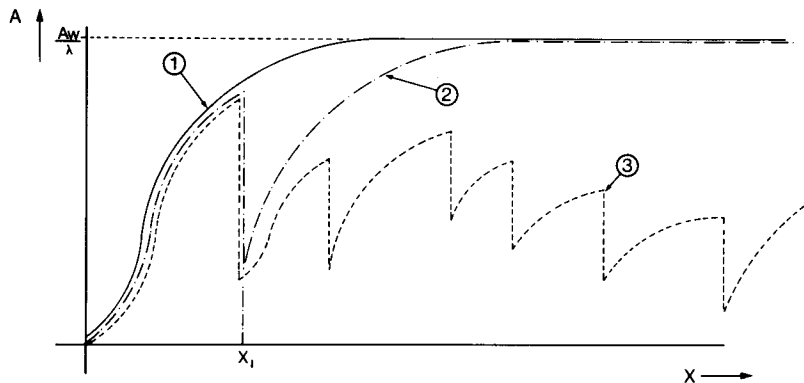
C. Theoretical profiles of radon activity in a long tubular cave. (1) Constant flow along the tube. (2) Effect of a tributary with lower radon concentration at x_1. (3) Effects of several tributaries.

FIGURE 3. Radon activities in Castleguard Cave, April 1980.

If mixing of the two air streams were immediate, the radon activity just downstream would be given by

$$A_1 = \frac{V_0 A_0 + (V_1 - V_0)A_t}{V_1} \quad (11)$$

where A_t is the activity of the tributary air and A_0 the activity of the main flow just upstream given by insertion of $x = x_1$ and $V = V_0$ in equation 10. The overall profile is shown in Figure 3c as a dashed line and is given by:

$$A(x) = \frac{A_w}{\lambda}(1 - e^{-\lambda(x - x_1)/V_1}) + A_1 e^{-\lambda(x - x_1)/V_1} . \quad (12)$$

Applying equation 11 to the sharp declines in radon activity measured at the P24 shaft and First Fissure Waterfall Rooms suggests that the tributaries there must be very large indeed, as much as the flow from the entrance in the case of the P24 shaft, and more than eight times the entrance flow for Waterfall Rooms, even if the tributary air contains no radon at all. Such large increases are not supported at all by the airflow measurements (Figure 2) and we interpret the irregular low values in Figure 3b as due to the plastic detectors being situated in the path of much smaller tributary airflows before they have been fully mixed with the main flow. We consider that the envelope curve of the higher points indicates the true trend of activity in the mixed airflow of the main passage. The long decline of radon activity in the central part of the cave must be due to tributaries distributed along its length, in the manner indicated by the dotted line in Figure 3c.

If numerous small tributaries are present, their effects can best be understood by supposing the simple tube of equation 10 to be replaced by one in which the velocity increases downflow at a rate k, due to entry of tributary air with radon activity A^*. If the air at $x = 0$ has activity A_0, then

$$A(x) = \frac{A_w + kA^*}{\lambda + k} \cdot \left\{ 1 - e^{-(\lambda + k)x/V} \right\}$$
$$+ A_0 e^{-(\lambda + k)x/V} \quad (13)$$

and

$$\frac{dA}{dx} = \frac{A_w + kA^*}{V} \cdot e^{-(\lambda + k)x/V}$$
$$- \frac{A_0(\lambda + k)}{V} \cdot e^{-(\lambda + k)x/V} \quad (14)$$

(Note that equation 10 is the special case of equation 13 when $k = 0$ and $A_0 = 0$.) From equation 14 we can see that radon activity will decrease in a downflow direction if A^* is less than A and,

$$k > \frac{A_w - \lambda A_0}{A_0 - A^*} . \quad (15)$$

If we could estimate the value of k for the central section of Castleguard Cave, the measured rate of discharge increase in Figure 2 would provide an independent check. We can obtain a minimum value of k by taking $A_0 = 10.7 \times 10^{-2}$ mm^{-2} h^{-1} equivalent to 8.3 pCi L^{-1}, the value at 4000 m from the entrance, and $A^* \approx 0$ (a greater value of A^* would imply a higher value for k). Unfortunately, we do not know the value of A_w and must either estimate it from the radon profile in another part of the cave or from a priori argument. We shall take the a priori argument first.

Andrews and Wood (1972) have shown that radon emanation occurs from crushed limestone particles by recoil of the nuclei into intercrystal cracks and crystal imperfections, followed by rapid diffusion to the particle surface. They demonstrate that radon is emanated from a layer only a few micrometers thick at the surface of the particle. We may apply reasoning based on Andrews and Wood's results to estimate the radon emanation into cylindrical cavities of various sizes. If the cavity wall has an emanation rate a_w (atoms per unit area per unit time), the rate of radon addition per unit volume of cavity will vary with the reciprocal of the cavity radius,

$$A_w = \frac{2a_w}{r} \cdot \lambda . \quad (16)$$

The value of a_w may be estimated from the ^{238}U content of the rock, with the assumptions that the decay series from ^{238}U to ^{226}Ra is in secular equilibrium and that all the radon produced by radioactive decay in a layer of thickness, d, adjacent to the wall is emanated into the cavity, while none of the radon produced at greater depths into the wall escapes. Then

$$A_w = \frac{2a_w\lambda}{r} = \frac{2}{r} \frac{C_{238} \, \rho \, d \, A_{238} \, \lambda}{3.7 \times 36} \text{ pCi m}^{-3} \text{ h}^{-1} \quad (17)$$

where C_{238} is the concentration of ^{238}U in micrograms per kilogram of rock, ρ is the rock density = 2600 kg m^{-3}, d is the emanating layer thickness $\sim 10^{-5}$ m (Andrews and Wood, 1972: Table 6), A_{238} is the specific activity of ^{238}U = 44.4 disintegrations per microgram per hour, and the other numbers are for conversion into picocuries and hours. For a ^{238}U concentration of 2.2×10^3 μg kg^{-1} (the world average for carbonates; Parker, 1967),

$$A_w = \frac{0.13}{r} \times 10^{-3} \text{ pCi L}^{-1} \text{ h}^{-1} . \quad (18)$$

Table 3 shows values for a_w calculated for different-sized cavities using equation 18. Also shown are the equilibrium radon concentrations at which emanation is just balanced by radioactive decay in different cavities (which must be the upper limiting value given by equation 10 as $x \to \infty$).

A second, more empirical estimation of A_w may be obtained by fitting equation 10 to the first few data points near the entrance in Figure 3b. With $V \approx 450$ m h^{-1} the

data of the first 2600 m imply that $A_w \approx 3.5 \times 10^{-2}$ mm^{-2} h^{-2}. Using Figure 3a, this figure may be converted to $A_w \approx 1.3$ pCi L^{-1} h^{-1}, over three magnitudes larger than the value suggested by Table 2. The discrepancy between these two estimates implies that almost all of the radon accumulating in the first part of the cave enters by some other mechanism than direct emanation from the cave wall. Although between 0 and 10 pCi L^{-1} ($\bar{X}$ = 2.9 pCi L^{-1} water, s = 3.4 pCi L^{-1}, n = 15) of radon is present in water entering the cave, and most of this is lost to the atmosphere by degassing, the total flux from this source is certainly small due to very low water discharge during the winter season when measurements were made. There is also no relation between water entry and rate of increase in radon down the passage. The higher value of A_w would suggest that the cave passage radon was derived from a porous region surrounding the cave. A cylinder of 20 to 40 m radius with rock porosity of 1% composed entirely of either cylindrical voids of 1 mm radius, or planar joints 2 mm wide, would suffice.

Table 2 suggests that voids of 1 mm radius or smaller will have radon concentrations from several tens to several hundreds of pCi L^{-1}. The rate of increase of radon track density in the first 1000 m of the cave is 7.8×10^{-2} mm^2 h^{-1} km^{-1} equivalent to 5.6 pCi L^{-1} km^{-1}. If this increase were entirely due to entry and mixing of air from cylindrical voids with 1 mm radius, the downflow increase in discharge required would be 0.13 m^{-3} s^{-1} km^{-1} or 17% of the discharge at the entrance. This is strikingly similar to the increase of 0.14 m^3 s^{-1} km^{-2} estimated from airflow measurements in Figure 2. However, it must be remembered that the measured increase of airflow is an average for the whole cave and may not apply to the first 1000 to 2600 m, and that the possible contribution of smaller voids with higher radon concentrations has been neglected. Nevertheless, the figures strongly suggest that most of the increase in radon concentration in the first part of the cave is due to either diffusion or advection of the gas from the submillimeter voids in the rocks around the cave.

Returning to the central section of the cave in which radon levels decline, we may use our estimates of A_w and equation 15 to show that, in the case where direct wall emanation is the sole radon source ($A_w = 0.71 \times 10^{-4}$ pCi L^{-1} h^{-1} for a cylindrical passage of 10.4 m^2 cross section), radon levels would decline even if k were zero. This is because such emanation rates are too small to compensate for the radioactive decay of radon in the air. If, on the other hand, the value of A_w is raised to about 1.3 pCi L^{-1} h^{-1} by the same process of diffusion or advection as seems to occur near the entrance, then a downflow decline in concentration requires at least 0.88 m^3 s^{-1} km^{-1} of radon-free tributary air, which is six times higher than the rate observed (Figure 2). We must conclude that the value of A_w is less in this section of the cave than in the entrance. If we take k = 0.014 m s^{-1} km^{-1} (from the measured discharge increase in Figure 2 of 0.14 m^3 s^{-1} km^{-1}, over a cross section of 10.4 m^2) then

TABLE 3
Specific radon emanation rates and equilibrium radon concentrations for long cylindrical voids[a]

Void radius (m)	A_w (pCi L^{-1} h^{-1})	$A = A_w/\lambda$ (pCi L^{-1})
10^{-4}	2.86	374
10^{-3}	2.86 × 10^{-1}	37.4
10^{-2}	2.86 × 10^{-2}	3.74
10^{-1}	2.86 × 10^{-3}	3.74 × 10^{-1}
1	2.86 × 10^{-4}	3.74 × 10^{-2}
10	2.86 × 10^{-5}	3.74 × 10^{-3}

[a]Thickness of rock layer emanating radon = 10^{-5}m; emanation efficiency = 100%; rock density = 2600 kg m^{-3}; ^{238}U content = 2.2 ppm.

$A_w < 0.11$ pCi L^{-1} h^{-1} or one-twelfth of its value near the entrance. Nevertheless, such a value would still require considerable diffusion or advection of radon from the rock around the walls.

Summary of Airflow Patterns

As we have seen, direct measurement suggests that air discharge increases along Castleguard Cave (Figure 2). This is confirmed by the patterns of radon activity (Figure 3b) which reveal the entry points of low-radon tributaries at P24 shaft, Waterfall Rooms (First Fissure), the Alley, A62 shaft, Waterfall Rooms (Second Fissure), and in the shaft-complex area around the Crutch. Some of these may connect via relatively open routes to known potholes in the area. In addition, the radon pattern suggests an entry by diffusion of radon gas or advection of radon-rich air from small voids between the entrance and First Fissure, with a smaller such influx in the central section of the cave. At this point it is necessary to anticipate the next section of this paper and refer to Figure 5a, in order to demonstrate that favorable conditions do exist in at least part of the cave for the entry of air from small voids in the walls (i.e., for an advective flux of radon into the cave as distinct from a diffusive flux). Figure 5a shows approximate isotherms of temperature in the rocks above the cave. It is clear that for the whole of the cave between the entrance and the Grottoes the mean temperature of the air column in the rocks above is less than that of the air column in the cave itself. Thus, the air in voids just above the roof will be at higher pressure than in the cave, due to the greater density of the cold air above (equation 1). This pressure difference will cause air to flow into the cave. Beyond the Grottoes the sign of the pressure difference is no longer obvious from Figure 5a as it depends more strongly on the unknown temperature distribution in the Columbia Icefield. In any event, the warmer rocks above the cave will produce less tendency for air to flow into the cave from small voids. The net effect of the temperature distribution will be to add more radon-rich air to the cave air in the section

before the Grottoes. This may account for the contrast in values of the radon addition rate, A_w, deduced from

Figure 3b for the central part of the cave compared with the first 2600 m.

THE THERMAL REGIME OF CASTLEGUARD CAVE

The air temperatures in the first half of the cave were measured in April 1973 and reported by Ford et al. (1976). In April 1979 and 1980 new temperature profiles were made as far as 4200 and 8100 m from the entrance. In April 1980 the temperature of the walls was also measured. The air profiles were made with sling-mounted mercury thermometers with wet and dry bulbs, read to ±0.2°C. Several instruments were used for each profile and were checked against each other before use. Wall temperatures were recorded, (1) by inserting the bulb and stem of a mercury-in-glass thermometer into a pencil-sized hole in cave sediments, or in sediment-filled cracks in rock, and (2), in the first 1500 m of the cave with a pinhead sized thermistor (precision, ±0.05°C) which was inserted into 1- to 3-mm-wide cracks. A few air temperatures were measured with the thermistor by suspending it in the center of the passage.

Air temperature profiles are presented in Figure 4a and wall temperatures in Figure 4b. They show that the cave contains a central warm section at 2.5 to 3.8°C between 2000 and 6700 m from the entrance. Temperatures in this section show only small variations from year to year, the 1979 and 1980 values agreeing closely with the 1973 data of Ford et al. (1976). What variation there is lies within the expected reading and calibration errors, as the thermometers used in one year were not checked against those used in the next.

In the first 2000 m of the cave, there are significant differences between 1979 and 1980 temperatures. Figure 4a shows that these year-to-year variations are matched by day-to-day differences between two profiles recorded on 19 and 20 April 1980. The differences between these two profiles reflect the diurnal temperature changes outside the cave. Thus, the first 2000 m comprise a dynamic zone in which changes in external temperature are felt on both daily and seasonal time scales.

Air temperature behavior in the dynamic zone of caves has been analyzed from a theoretical standpoint by Wigley and Brown (1971). They show that for a cave with walls at constant temperature the difference between the walls and air blowing into the entrance is reduced to a fraction $1/e$ of its initial value within a "relaxation length," x_0. The air reaches approximately the same temperature as the walls within 4 to 5 relaxation lengths. The relaxation length depends only on the radius of the cave (for circular cross section) and air velocity, and an appropriate value for Castleguard Cave is $x_0 \approx 300$ m (from Wigley and Brown, 1971, Figure 1). The dynamic zone observed in Castleguard is 6 to 7 times x_0, slightly more than suggested by theory. The discrepancy may be explained by the fact that the cave wall temperatures vary both with distance from the entrance and probably also with time (Figure 4b). Both these factors will tend to increase the

penetration of surface temperature differences into the cave.

In 1979 air temperatures in the first 400 m of the cave showed a minimum value which was colder than the outside air at the time (Figure 4a). Wigley and Brown's (1972) theoretical calculations suggest that air entering a warmer cave will cool initially due to evaporation of moisture from the walls. Alternatively, it may simply reflect very low rock temperatures which are in part induced by the cold winter air current blowing into the entrance.
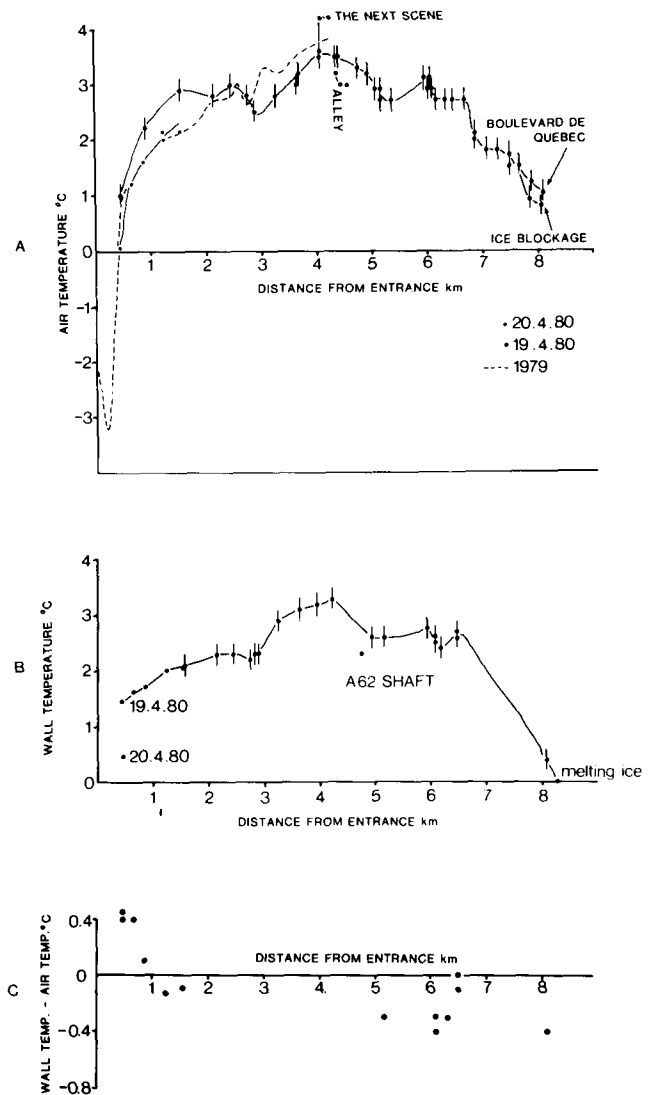
FIGURE 4. The thermal regime in Castleguard Cave. A. Air temperatures. B. Wall temperatures. C. Difference in air and wall temperatures (measured on the same occasion).
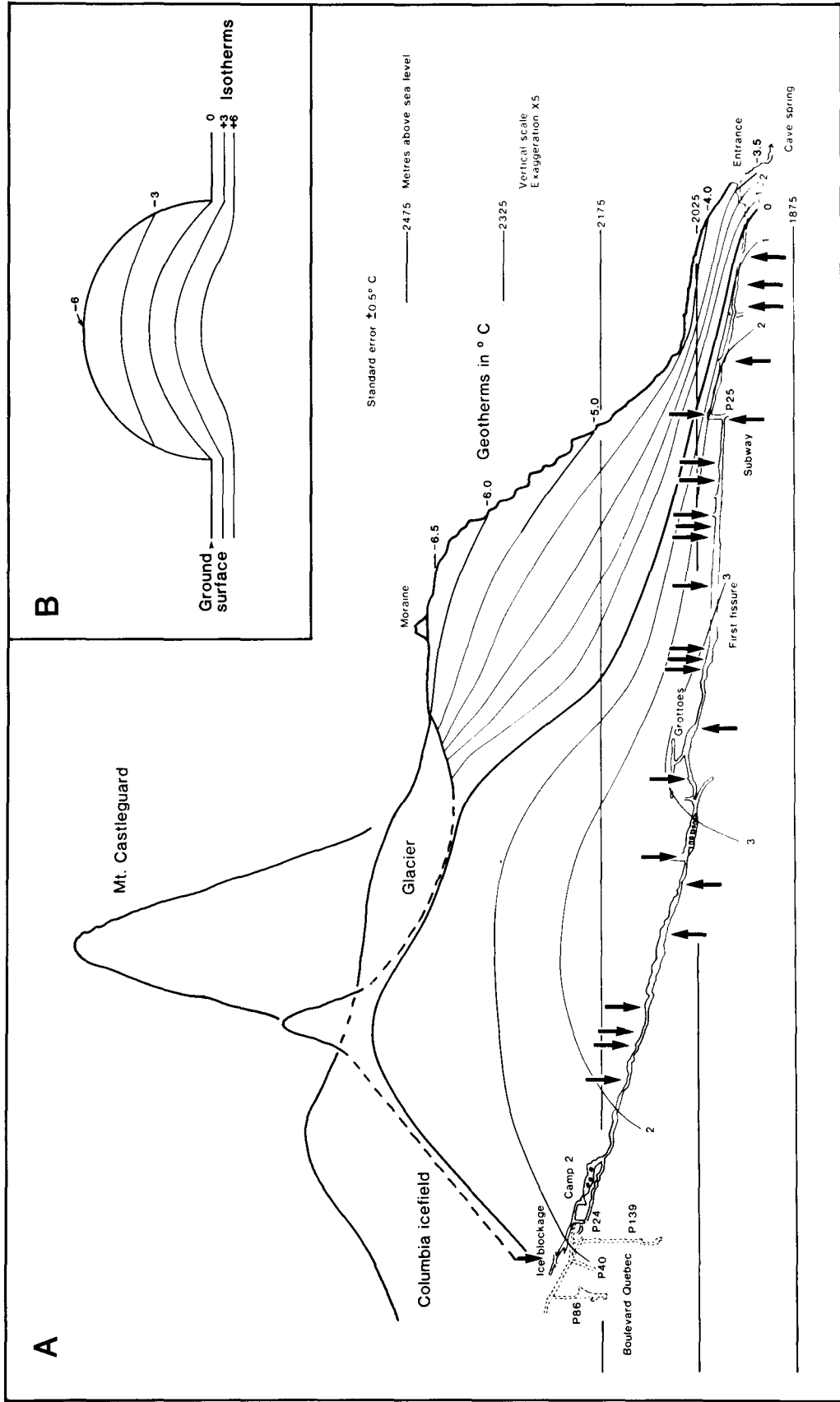
FIGURE 5. A. Geoisothermal section of Mount Castleguard and the cave, inferred from data of Figure 4 and Table 1. B. Relative temperature distribution in an idealized semicylindrical ridge, calculated from heat flow theory.

In the thermally stable central section of the cave there is a general increase in temperature to around 3.5°C at 4000 to 4500 m from the entrance, then a decline to 6700 m. Superimposed on the general trends are local anomalies of colder air, which are also seen in the wall temperature profile. The most prominent are at 3000 m, 5000 to 6000 m, 6100 m, and 6800 to 7200 m from the entrance (Figure 4) and coincide with points at which low radon activities indicate the entry of air from fissure-sized voids (Figure 3). This suggests that cold tributary air cools the main flow, and that the tributary air itself is derived from cold rocks above the cave or possibly from fairly direct connections via fissures to the surface.

From around 6700 m to the end of the known cave, air temperature declines from more than 2.5 to less than 1°C. Wall temperatures show an even greater decline to 0.4°C at 150 m from the Ice Blockage. Slight melting of the Ice Blockage itself suggests that wall temperature there is ca. 0°C. Temperatures in this section of the cave may be affected by the dynamic zone effects of summer airflow, which must enter from the Columbia Icefield at about 0°C and may chill the walls of the first 2000 m or so of passages. Conversely, the walls are likely to be warmed in winter by air blowing from the central section. If seasonal effects have any importance at all, temperatures in the final section should be at a maximum towards the end of winter when the measurements of Figure 4 were made. These considerations suggest that the general cooling from 6700 m to the end of the cave is a persistent pattern, probably due to the general geothermal gradient in the bedrock towards the base of the icefield, although the precise temperatures may vary seasonally.

Most caverns in regions of moderate relief possess a dynamic zone of changing temperatures close to the entrance, and an internal zone with nearly constant temperature which is close to the mean annual temperature at the surface. In the alpine situation of Castleguard, this would require the central section of the cave to be at around –4°C, equal to mean annual temperature near the level of the entrance. In fact, the cave air is much warmer than this, averaging 3°C in the central section and 2.4°C in the whole of the known cave. Wall temperatures average 2.7°C in the central section and 2.3°C in the whole cave beyond 400 m from the entrance. The only conceivable source of heat to maintain the cave at these temperatures is geothermal. In Figure 5a isotherms are drawn based on measured wall and air temperatures from Figure 4, calculated surface temperatures based on Table 1, and an assumed basal temperature of ca. 0°C for the Columbia Icefield.

Two features of Figure 5 are important. First, the warm central section of the cave and the convex-upward isotherms are entirely to be expected in a heatflow field dominated by heat conduction through rocks. Figure 5b shows the theoretical temperature pattern in an idealized semicylindrical ridge, obtained by solving the Laplace equation for heat conduction for a horizontal cylinder whose surface temperature conforms to the geothermal gradient in its lower half and to the atmospheric lapse rate in its upper half. A convex-upward pattern of isotherms is apparent, giving the ridge a warm core relative to surface temperatures at the same level, just as is seen in Castleguard Cave. Second, the real-world isotherms of Figure 5a are asymmetrical, with a much smaller geothermal gradient towards the icefield than towards the icefree side of the mountain despite the uniform conductive heat flux which it is reasonable to suppose exists at depth throughout the area. This is largely a consequence of the chosen boundary conditions, but these are believed to be realistic, and the asymmetry is believed to be real. It cannot be due simply to the presence of the icefield as an insulating layer, as thermal conductivities of carbonate rock and ice are approximately equal. The most probable explanation of the asymmetry is that meltwaters from the glaciers abstract heat as they pass downwards through fissures. Since the geothermal gradients due to conduction alone should be equal on both sides of the mountain (Figure 5b), and the gradients on Figure 5a vary by a factor of 3 from 0.02°C m^{-1} to 0.007°C m^{-1}, we conclude that the reduction of conductive heat flux by meltwaters amounts to two-thirds of the total. Ford et al. (1976) reached a similar conclusion and cite the temperature of 2.2°C achieved by meltwaters in Big Springs as independent evidence of the downward advection of heat.

EVAPORATION, CONDENSATION, AND HEAT EXCHANGE

Figure 6 shows the vapor pressure and relative humidity of the air in Castleguard Cave. The vapor pressure profiles closely resemble the temperature profiles (Figure 4a) because, through most of the cave, the relative humidity exceeds 97%, so the vapor pressure is primarily a function of dry-bulb temperature. Under the winter conditions studied, three zones can be distinguished on Figure 6. In the first 1300 m of cave the relative humidity increases rapidly to near 100% and vapor pressure rises from ca. 5 to ca. 7 mb. This is a zone of vigorous evaporation, which explains the presence of ablation sculpturing of ice in the first 450 m, dry walls and sediments up to 1200 m (Figure 7), and bladed forms of calcite "popcorn" speleothems growing along joint traces in the walls and on the windward edges of rock surfaces (White, 1976; Harmon et al., 1983, this symposium). Although most of the walls are dry there are some pools and these, together with slow seepage from joints, form the source of the moisture.

The second zone of Figure 6 extends from 1200 to 4500 m from the entrance. The vapor pressure increases roughly linearly at average rates between 2.5 to 4.4 × 10^{-4} mb m^{-1}, with local zones of lower moisture content corresponding to the local cooling discussed above. Rela-

tive humidity reaches 100% in the parts of this zone where moisture enters, but is significantly below 100% for long sections in which cave walls and sediments are dry and crumbly and there is abundant growth of gypsum and evaporite minerals (Harmon et al., 1983, this symposium). In these parts, the supply of moisture from the walls is presumably insufficient to match the rate of warming of the air. Finally, the third zone extends from 4500 m to the end of the cave. Vapor pressure shows a fairly constant decline at 4.2 to 5.2 × 10^{-4} mb m^{-1} with locally more rapid decline corresponding to the entry of colder (and hence drier) air revealed by temperature and radon profiles. Throughout this zone the walls are mostly damp and condensation appears on apparatus such as radon detectors left in place for more than a few hours. Part of the Second Fissure does show gypsum and evaporite mineral development and it is thought that this may be due to evaporation by the reversed cave wind in summer. In winter, relative humidity is 100% throughout.

The changes of temperature and humidity along the cave appear to be due largely to heat and vapor exchange with the walls. Nevertheless, some features, such as the cooling from 4500 m to the cave's end, could conceivably be explained by other factors. Adiabatic expansion of saturated air over the cave's height range of 350 m should cause cooling by around 2°C which might explain part of the observed pattern. However, the following discussion demonstrates that heat exchange with the walls in fact predominates in determining the observed temperature profile.

We may describe the evolution of a small volume of air as it passes along the conduit by three conservation equations,

$$\text{Mass:} \quad \frac{d}{dt}(\rho V r^2) = 0 \qquad (19a)$$

$$\text{Moisture:} \quad \frac{d}{dt}(\rho V r^2 q) = \rho S V r^2 \qquad (19b)$$

$$\text{Heat:} \quad \frac{d}{dt}(\rho V r^2 T c_p) = -\rho V r^2 \{c_p \Gamma_{ad} \sin \Theta - H\} \qquad (19c)$$

in which q is the specific humidity; S is a moisture source or sink expressed as mass of water added per unit time to unit mass of air; T is temperature (°K); c_p is the specific heat of air at constant pressure; Γ_{ad} the adiabatic lapse rate; Θ the slope of the cave passage, and H a heat source or sink expressed as heat gained per unit time per unit mass of air. The term H includes both latent and sensible heat transfer, given by

$$H_{lat} = -LS \qquad (20a)$$

and

$$H_{sen} = \frac{2k}{\rho r}(T_w - T) \qquad (20b)$$

where L is the latent heat of evaporation; k the heatflow per unit time across unit area of cave wall per unit difference in temperature, and T_w is the surface temperature of the cave wall. If ρ is approximately constant with distance along the cave passage (x), which is true if the total height range is small, and if $V = dx/dt$ is approximately constant, then equations 19 and 20 can be combined to give

$$\frac{dT}{dx} = -\Gamma_{ad} \sin \Theta + \frac{2k}{\rho r} \cdot \frac{1}{Vc_p}(T_w - T)$$

$$- \frac{L}{c_p} \cdot \frac{dq}{dx} \qquad (21)$$

Since $\Gamma_{ad} = -dT_{ad}/dz$, where T_{ad} is the dry adiabatic lapse rate temperature, we have

$$\frac{d}{dx}(T - T_{ad}) = \frac{2k(T_w - T)}{\rho r V c_p} - \frac{L}{c_p}\frac{dq}{ds} \cdot \qquad (21a)$$
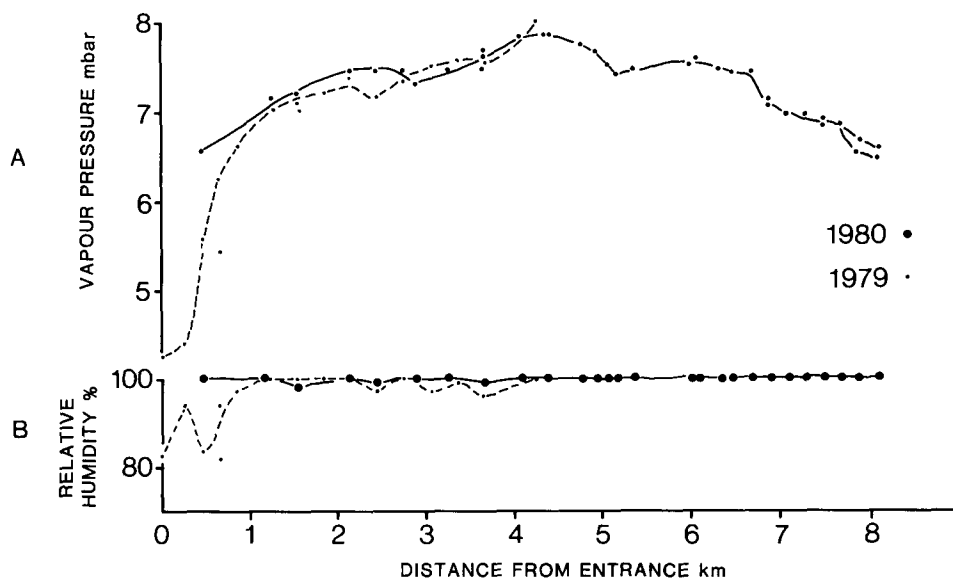
FIGURE 6. Vapor pressure and relative humidity of the air in Castleguard Cave.

For saturated air,

$$\frac{dT_{ad}}{dx} - \frac{L}{c_p}\frac{dq}{dx} = \frac{dT_{as}}{dx} \qquad (22)$$

where T_{as} is the saturated adiabatic lapse rate temperature. Combining (21a) and (22) gives

$$\frac{d}{dx}(T - T_{as}) = \frac{2k(T_w - T)}{\rho r V c_p} \qquad (23)$$

which expresses the fact that the difference in temperature between the saturated cave air and similarly saturated air following the vertical adiabatic lapse rate outside is due to sensible heat exchange with the cave walls. Equation 23 is formally homologous with the equation

A. Late winter (April) conditions when outside air flows in from the mouth. Residual flood waters are frozen solid. All rock and ice surfaces are dry and bare.

B. In summer (early July) conditions, just before the first summer floods. Air is flowing out from the moist interior of the cave. All surfaces are coated with hoarfrost.

FIGURE 7. Castleguard Cave entrance passage, 50 m from the cave mouth.

for humidity change in a conduit with constant wall temperature presented by Wigley and Brown (equation 7, 1971). It may be simplified by adopting as a length scale the relaxation length

$$x_0 = \frac{\rho r c_p V}{2k}$$

and defining $X = x/x_0$

which yields

$$\frac{d}{dX}(T - T_{as}) = T_w - T. \qquad (23a)$$

This may be rewritten to express the influence of cave slope explicitly by using

$$T_{as} \approx T_0 + \Gamma_{as} z \qquad (24)$$

where T_0 is the temperature at the cave entrance. Therefore,

$$\frac{dT}{dX} - \Gamma_{as}\frac{dz}{dX} = \frac{dT}{dX} - \Gamma_{as}x_0 \sin \Theta = T_w - T \quad (25)$$

which gives

$$\frac{dT}{dX} > 0 \text{ when } T_w - T > -\Gamma_{as} x_0 \sin \Theta \qquad (26)$$

For the first half of Castleguard Cave, $x_0 \approx 300$ m and $\sin \Theta \approx 1/40$. With $\Gamma_{as} = -0.006°C$ m^{-1}, equation 26 predicts that the cave air will experience net warming (i.e., the effects of moist adiabatic cooling will be outweighed by heat transfer from the walls) providing that the walls

are more than 0.05°C warmer than the air. If the temperature difference is smaller than this the warming will be insufficient to offset adiabatic cooling. In the second half of the cave, $\sin \Theta \approx 1/25$ and cooling of the air occurs when $T_w - T < 0.07°C$. In fact, as Figure 6c shows, the actual differences between wall and air temperatures are an order of magnitude greater than this, indicating that both warming and cooling trends are primarily due to heat exchange with the cave walls.

The apparent latent and sensible heat fluxes from the walls can be calculated from the data of Figures 4 and 6 using the equations

$$H_{lat} = -L\rho Q\,\frac{dq}{dx} \approx -\frac{0.622\,L\rho Q}{p}\,\frac{de}{dx} \quad (27a)$$

where the minus sign indicates that evaporation cools the air, and

$$H_{sen} = C_p\rho Q\,\frac{dT}{dx} \qquad (27b)$$

where Q is the air discharge rate and e the vapor pressure.

Table 4 shows calculated values of both latent and sensible heat transfer based on linear regressions fitted through appropriate groups of points on Figures 4a and 6a. Units are joules per second per meter. Also shown are the equivalent evaporation rates of a uniform film of water from the walls of a circular conduit with a cross section of 10.4 m^2, in units of millimeters of water per year. Evaporation of seepage from the walls is suspected to be responsible for the precipitation of most of the more unusual minerals found in the cave, and perhaps for some calcite deposition also (Atkinson, 1983, this symposium; Harmon et al., 1983, this symposium). The very low values in Table 4 suggest that such mineral growth will be extremely slow.

CONCLUSIONS

Because of its simple layout, considerable length, and alpine setting, Castleguard Cave provides an excellent opportunity to study chimney-effect winds. A simple theory of such winds predicts the cave's actual behavior

TABLE 4

Heat and water vapor transfer rates

Region	Vapor pressure gradient (mb m^{-1})	Temperature gradient (°C m^{-1})	Sensible heat transfer (J s^{-1} m^{-1})	Latent heat transfer (J s^{-1} m^{-1})	Evaporation rate (mm yr^{-1})
1979 Data					
0–1200 m	$\approx 2.5 \times 10^{-3}$				≈ 14
1200–4200 m	2.5×10^{-4}	6.2×10^{-4}	0.09	0.07	1.4
1980 Data					
1200–4200 m	4.4×10^{-4}	8.8×10^{-4}	0.13	0.12	2.5
4200–5500 m	-4.2×10^{-4}	-7.3×10^{-4}	-0.10	-0.12	-2.2
6000–8200 m	-5.2×10^{-4}	-1.0×10^{-3}	-0.14	-0.14	-2.8

fairly well, giving consistent values of the friction factor, f, in the range 0.8 to 2.3 under different conditions. After allowing for the effect of constrictions, the friction factor for Castleguard Cave is shown to be somewhat higher than values for rough mine galleries, in the range 0.3 to 0.9. This is the first time that true values of f have been estimated for cave conduits with reasonable precision, and it is hoped that they will prove useful in future studies in water and air flow in caves.

Radon levels measured in Castleguard Cave are in the range 1 to 10 pCi L^{-1}. While lower than the levels found in single-entrance caves (Ahlstrand, 1980) these values are much greater than could be accounted for by emanation from the cave walls alone. They indicate that, even in a simple system such as this, tributary air currents occur from fissures and possibly also from smaller voids in the rock. Radon is advected or diffuses into the cave from a large volume of rock around it, and future studies of cave meteorology should not assume that the walls behave impermeably, as has commonly been the case in the past. We know of one other instance where the pores in the rock matrix surrounding a cave have been shown to contribute significantly to the flow of air in the main conduit. This is the case for many of the caves in the Nullarbor Plain of southern Australia. Here the caves "breathe" in response to variations in atmospheric pressure, and the large magnitude of the air flow and the fact that changes in flow direction lag behind changes in the sign of the rate of change of pressure can only be explained if the caves are considered as conduits embedded in a porous rock matrix (Wigley, 1967).

Castleguard Cave affords an opportunity to measure a near-horizontal temperature profile through rocks overlain by glaciers. The thermal regime shows that the Castleguard Mountain massif possesses a warm core due to a geothermal heat flow, as would be expected by theory. Also indicated is an approximately two-thirds reduction in geothermal heat flux towards the soles of the glaciers. This seems to be due to downward abstraction and advection of heat by meltwaters. Similar effects could be important beneath other glaciers on permeable rocks in mountainous terrain.

The warming and cooling of the cave air has been demonstrated to be due predominantly to heat exchanges with the walls. Thus the cave provides a qualitative test for Wigley and Brown's (1971) theory of heat and vapor exchange effects, although the cave's thermal regime does not exactly match the conditions assumed by the theory. Castleguard Cave has a dynamic zone of similar length to that predicted by the theory, and a cold zone close to the entrance may possibly be due to evaporative cooling, as suggested by the theory.

Evaporation rates in Castleguard Cave are measurable, but extremely low except in the dynamic zone close to the entrance. Their low values suggest that evaporite minerals would take a long time to form. Nevertheless, there is good agreement between the occurrence of evaporites and sections of the cave where evaporation is occurring and relative humidity is sometimes less than 100%.

ACKNOWLEDGMENTS

REFERENCES CITED

Ahlstrand, G. M., 1980: Alpha radiation levels in two caves related to external air temperature and atmospheric pressure. *National Speleological Society of America Bulletin,* 42: 39–41.

Andrews, J. N. and Wood, D. F., 1972: Mechanism of radon release in rock matrices and entry into groundwaters. *Transactions Institute of Mining and Metallurgy,* Section B (811): 180–209.

Atkinson, T. C., 1977: Diffuse flow and conduit flow in limestone terrain in the Mendip Hills, Somerset (Great Britain). *Journal of Hydrology,* 35: 93–110.

———, 1983: Growth mechanisms of speleothems in Castleguard Cave, Columbia Icefields, Alberta, Canada. *Arctic and Alpine Research,* 15: 523–536.

Ford, D. C., Harmon, R. S., Schwarcz, H. P., Wigley, T. M. L., and Thompson, P., 1976: Geo-hydrologic and thermometric observations in the vicinity of the Columbia Icefield, Alberta and British Columbia, Canada. *Journal of Glaciology,* 16(74): 219–230.

Ford, D. C., Smart, P. L., and Ewers, R. O., 1983: The physiography and speleogenesis of Castleguard Cave, Columbia Icefields, Alberta, Canada. *Arctic and Alpine Research,* 15: 437–450.

Harmon, R. S., Atkinson, T. C., and Atkinson, J. L., 1983: The mineralogy of Castleguard Cave, Columbia Icefields, Alberta, Canada. *Arctic and Alpine Research,* 15: 503–516.

Henshaw, D. L., Fews, A. P., and Webster, D. J., 1979: A technique for high sensitivity alpha autoradiography of bronchial epithelium tissue. *Physics in Medicine and Biology,* 24: 1227–1242.

McElroy, G. C., 1966: Mine ventilation. *In* Peele, R. (ed.), *Mining Engineers Handbook I.* 3rd edition. New York: John Wiley.

Parker, R. L., 1967: Data of geochemistry: Chapter D. Composition of the earth's crust. *U.S. Geological Survey Professional Paper,* 440-D. 17 pp.

Streeter, V. L., 1971: *Fluid Mechanics.* 5th edition. New York: McGraw-Hill. 751 pp.

Wigley, T. M. L., 1967: Non-steady flow through a porous medium and cave breathing. *Journal of Geophysical Research,* 72: 3199–3205.

Wigley, T. M. L. and Brown, M. C., 1971: Geophysical applications of heat and mass transfer in turbulent pipe flow. *Boundary Layer Meteorology,* 1: 300–338.

————, 1976: The physics of caves. *In* Ford, T. D. and Cullingford, C. H. D. (eds.), *The Science of Speleology.* London: Academic Press, 329–358.

White, W. B., 1976: Cave minerals and speleothems. *In* Ford, T. D. and Cullingford, C. H. D. (eds.), *The Science of Speleology.* London: Academic Press, 267–328.